Theor Chem Acc (2001) 105:244–251
DOI 10.1007/s002140000205

Theoretical
Chemistry Accounts

Regular article

A reexamination of virial coefficients of the Lennard-Jones fluid

Kippi M. Dyer, John S. Perkyns, B. Montgomery Pettitt

Chemistry Department, University of Houston, Houston, TX 77204-5641, USA

Received: 31 July 2000 / Accepted: 18 September 2000 / Published online: 21 December 2000

Abstract. The fourth-order virial coefficients have been calculated exactly to five decimal places for pure fluids of the Lennard-Jones potential at many points in the phase diagram. The calculations were performed through direct evaluation of the integrals, or diagrams, which make up the density expansion of the radial distribution function: included were the standard fast Fourier transform method of evaluating the simply connected diagrams and the evaluation of the bridge diagram for the fourth order in density by expansion in Legendre polynomials. The polynomial-order dependence of the bridge diagram calculation and the range dependence of the simply connected diagrams of the fourth order are found to have more significance than was thought from previous studies, especially in the low-temperature range. This result was confirmed by direct evaluation of the diagrams which construct the virial coefficients, as given by Rowlinson, Barker, and coworkers. This calculation confirmed that numerical convergence has not been achieved at the precision levels previously reported in the literature. These differences, though minor at higher temperatures, can be seen to be more significant at the lower temperature ranges.

Key words: Bridge diagrams – Phase diagrams – Numerical convergence

1 Introduction

The virial equation of state for gases has been used in a variety of engineering applications, such as turbine design, steam tables, and general applications which require knowledge of the deviations from the ideal gas law for a particular industrial application [1, 2, 3]. The noble gases and other monatomic gases give us the most reasonable of the model systems by which we may theoretically study the virial equation, as well as one which could, at least in principle, be extended to more complex systems such as water.

In its simplest form the virial equation of state can be written

$$\frac{\beta P}{\rho} = 1 + B\rho + C\rho^2 + D\rho^3 + \cdots \quad ,$$

where P is the system pressure, ρ is the number density of a pure species, and $\beta = 1/kT$, with T the absolute temperature and k the Boltzmann constant. The scalar quantities B, C, and D are known as the second, third, and fourth virial coefficients, respectively.

Historically, the virial equation has been a focus of statistical mechanical theory [1, 4, 5]. In particular, much time and energy have been expended on attempts to calculate this equation of state from the knowledge of intermolecular forces [6, 7, 8, 9, 10] through an exact series of integrals written in terms of the potential and thermodynamic state variables. Necessary to the calculation of the equation of state by this route is the evaluation of the virial coefficients in terms of these integrals. The virial coefficients may also be written in terms of density-independent-component probability density functions, which themselves form a virial series summing to the radial distribution function. Thus, a solution for the components of the radial distribution function at each order of density will lead directly to the virial coefficient for the corresponding term in the virial equation [1, 4, 5, 6, 7, 8]. We will calculate the virial coefficient of fourth order and show that precise results can be achieved with a Legendre expansion of the bridge functions in reasonable computing times.

In this work, the calculation of virial coefficients is, therefore, broken down into the evaluation of function-valued integrals which combine to form the components of the radial distribution function. These integrals are sometimes represented by, and referred to as, diagrams. The diagrams are relatively few in number, and most can be evaluated simply using Fourier methods. There is one diagram, which is a component of the fourth virial coefficient, which must be evaluated directly as a

Correspondence to: B. M. Pettitt
e-mail: pettitt@uh.edu

six-dimensional integral. In recent closely related work by Perkyns and Pettitt [10], with the aim of calculating more accurate distribution functions for the liquid state from integral equations, a method was applied using expansion in Legendre polynomials developed by Attard and Patey [2]. The radial distribution components formed by adding subsets composed of this bridge diagram and the convolution diagrams become, in turn, components of the integrand in standard expressions for the virial coefficients. The resulting combination of polynomial expansion methods, the Gaussian integration of these expansions, and efficient fast Fourier transform (FFT) techniques shows itself to be computationally efficient.

A similar method of calculating the virial coefficients directly as scalar-valued diagrams was employed over 30 years ago by Barker and coworkers [6, 7, 8]. This method has been applied more recently by Sun and Teja [11]. This method yielded results for the Lennard-Jones fluid up to fifth order in density. Calculation by the current method, using strenuous numerical precision tests, will demonstrate that the error estimates in the literature were somewhat optimistic. We should state that the methods used by Barker and coworkers to calculate the second- and third-order virial coefficients were quite reasonable and that reproduction of their results using the modern FFT techniques is a straightforward procedure. For this reason we focus upon the more enigmatic fourth-order calculation in this work. To this end, and to show that the converged results are independent of the particular technique, we will also calculate the fourth-order virial coefficients directly, through the method given by Barker and coworkers. Recalculating the older literature data gives us a touchstone with which to directly compare the computational efficiency of the new method, as well as showing that the precision previously reported may be overstated.

One element necessary to the application of the techniques which we utilize here is the choice of a suitable intermolecular potential functional form. For this purpose we choose the Lennard-Jones 6-12 potential, which, while it has not proven to be the "best" potential for modeling monatomic gases, does provide useful insight into such systems while remaining analytically convenient. This potential form has been seen in quite a large body of computational studies, and thus its properties are well known [3]. Another aspect of the Lennard-Jones potential which makes it useful for this calculation is that it has been used for our purpose before by Barker and coworkers [6, 7] and by Sun and Teja [11].

This article has the following form. In Sect. 2 we show the formalism which we use to relate the radial distribution function, the integral equations, and the virial coefficients. We outline the method used to calculate the bridge diagram, give a brief description of the analytic expansion of the virial coefficients as used by Rowlinson [12], Barker and coworkers [6, 7, 8], and Sun and Teja [11] and conclude the section with a brief discussion of the equivalence of the two methods. Section 3 gives the results from our calculation, as well as a comparison of our results with those in the literature. The conclusions are presented in Sect. 4.

2 Theory

2.1 The radial distribution function and the virial coefficients

A standard expression for the equation of state of a simple fluid can be written as follows [4]:

$$\frac{\beta P}{\rho} = 1 - \frac{\beta}{3N}\left\langle \sum_{i=1}^{N} \mathbf{r}_i \cdot \nabla_i V_N(\mathbf{r}^N) \right\rangle \ , \tag{1}$$

where N is the number of particles, $\mathbf{r}_i$ is the radial distance vector for each particle i, P is the pressure of the system, ρ is the number density, and $-\nabla_i V_N(\mathbf{r}^N)$ is the force on each particle i. The angled brackets represent the ensemble average of the summation. Following standard methods [4], we introduce the radial distribution function, $g(r)$, which allows us to reduce this equation to a more tractable form,

$$\frac{\beta P}{\rho} = 1 - \frac{2}{3}\pi\beta\rho \int_0^\infty r^3 g(r) \frac{\mathrm{d}u(r)}{\mathrm{d}r}\mathrm{d}r \ , \tag{2}$$

for a given radially dependent, pairwise-additive intermolecular potential $u(r)$. The purpose of this substitution is to shift the difficulty of calculation away from the N-body sum present in the ensemble-averaged quantity in Eq. (1) to the determination of $g(r)$, a one-dimensional function of the interparticle separation $r \equiv r_{12}$. We simplify the problem further by classifying and separating the terms of $g(r)$ in terms of the Mayer f bond according to orders of density, i.e.

$$g(r) = \mathrm{e}^{-\beta u(r_{12})}\left[(1 + \rho g_1(r_{12}) + \rho^2 g_2(r_{12}) + \cdots\right] \ , \tag{3}$$

where $g_1(r_{12})$ and $g_2(r_{12})$ are given by the following

$$g_1(r_{12}) = \int f(r_{13}) f(r_{23}) \mathrm{d}\mathbf{r}_3 \ , \tag{4}$$

$$\begin{aligned} g_2(r_{12}) = & \int f(r_{13}) f(r_{34}) f(r_{42}) \mathrm{d}\mathbf{r}_3\, \mathrm{d}\mathbf{r}_4 \\ & + \frac{1}{2}\int f(r_{13}) f(r_{32}) f(r_{14}) f(r_{42}) \mathrm{d}\mathbf{r}_3\, \mathrm{d}\mathbf{r}_4 \\ & + 2\int f(r_{34}) f(r_{23}) f(r_{13}) f(r_{42}) \mathrm{d}\mathbf{r}_3\, \mathrm{d}\mathbf{r}_4 + d_3(r_{12}) \ . \end{aligned} \tag{5}$$

The last term in Eq. (5), $d_3(r_{12})$, represents a bridge function or diagram, which we will define later.

This expansion is convenient not only for the simplification of terms, but also for the logical conclusion that each term in the $g(r)$ expansion (Eq. 3) can be directly linked to the corresponding virial coefficient, B, C, and D, through the density ordering in the equation

$$\frac{\beta P}{\rho} = 1 + B\rho + C\rho^2 + D\rho^3 + \cdots \ . \tag{6}$$

We should also state here that the virial equation does not converge in so few terms for nongaseous states, but

while it may not do so, information important to many applications may still be extracted from the dominant terms in the series [1].

2.2 Diagrammatic expansion of $g(r)$

We now briefly outline the use of cluster diagrams as they pertain directly to the current calculation. Cluster diagram use and notation have been extensively examined in the literature [4, 6, 7, 8, 10, 12]; here we will state only that cluster diagrams are constructed from open circle root points, which represent spatial variables which are not integrated over, filled circle field points, which are variables integrated over, and bonds or functions, which in our case are the f bonds described previously. The expansion of Eq. (3) in terms of these diagrams is given in Fig. 1.

This diagrammatic expansion displayed in Fig. 1 suggests simplifying the integrals into the following

$$g_1(r_{12}) = f * f \ , \tag{7}$$

$$g_2(r_{12}) = d_1(r_{12}) + d_2(r_{12}) + d_3(r_{12}) \ , \tag{8}$$

where

$$d_1(r_{12}) = f * f * f \tag{9}$$

and

$$d_2(r_{12}) = \frac{1}{2}(f * f)(f * f) + 2f * [f(f * f)] \ . \tag{10}$$

Here $f = f(r_{12}) = \mathrm{e}^{-\beta u(r_{12})} - 1$ is the Mayer f bond [13], which is equivalent in all positions in a diagram representing a monatomic, spherically symmetric system such as we consider, and $*$ represents a convolution integral. Such convolution integrals are straightforward

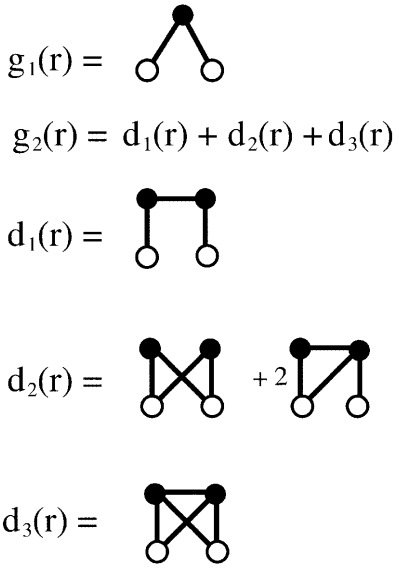

Fig. 1. The diagrammatic expansion of $g_1(r_{12})$ and $g_2(r_{12})$. The diagrams in the second, third, and fourth rows which sum to give $g_2(r_{12})$ represent $d_1(r_{12})$, $d_2(r_{12})$, and $d_3(r_{12})$, respectively

to calculate with the use of FFT, a technique which has been used with much success in this context [4, 6, 7, 8].

Once the diagrams have been calculated, the virial coefficients themselves are obtained using the equations

$$B = -2\pi \int_0^\infty r_{12}^2 f(r_{12}) \mathrm{d}r_{12} \ , \tag{11}$$

$$C = \frac{-2\pi\beta}{3} \int_0^\infty r_{12}^3 g_1(r_{12}) \frac{\partial u(r_{12})}{\partial r_{12}} \mathrm{d}r_{12} \ , \tag{12}$$

$$D_1 = \frac{-2\pi\beta}{3} \int_0^\infty r_{12}^3 d_1(r_{12}) \frac{\partial u(r_{12})}{\partial r_{12}} \mathrm{d}r_{12} \ , \tag{13}$$

$$D_2 = \frac{-2\pi\beta}{3} \int_0^\infty r_{12}^3 d_2(r_{12}) \frac{\partial u(r_{12})}{\partial r_{12}} \mathrm{d}r_{12} \ , \tag{14}$$

$$D_3 = \frac{-2\pi\beta}{3} \int_0^\infty r_{12}^3 d_3(r_{12}) \frac{\partial u(r_{12})}{\partial r_{12}} \mathrm{d}r_{12} \ , \tag{15}$$

and

$$D = D_1 + D_2 + D_3 \ . \tag{16}$$

The bridge diagram (function) labeled $d_3(r_{12})$ in Eqs. (5), (8), and (15) has proven to be the most difficult of the diagrams to calculate. This difficulty arises because it is impossible to reduce this diagram (the final diagram in Fig. 1) to the convolutions and multiplications with which we express the more simply connected diagrams. The calculation of $d_3(r_{12})$ in other contexts has been detailed explicitly in two sources [2, 7]; here we will give the necessary information for our purposes, and we refer the interested reader to the more detailed accounts. In analytic form, $d_3(r_{12})$ is expressed by

$$\begin{aligned} d_3(r_{12}) &= \frac{1}{2} \int f(r_{13}) f(r_{14}) f(r_{23}) f(r_{24}) f(r_{34}) \mathrm{d}\mathbf{r}_3 \, \mathrm{d}\mathbf{r}_4 \\ &= \pi \int_0^\infty r_3^2 \, \mathrm{d}r_3 \int_0^\infty r_4^2 \, \mathrm{d}r_4 \int_0^\pi \sin\theta_3 \, \mathrm{d}\theta_3 \int_0^\pi \sin\theta_4 \, \mathrm{d}\theta_4 \\ &\quad \times \int_0^{2\pi} f(r_{13}) f(r_{14}) f(r_{23}) f(r_{24}) f(r_{34}) \mathrm{d}\phi_{34} \ , \end{aligned} \tag{17}$$

where $\mathbf{r}_1$ is chosen as the origin and $\mathbf{r}_2$ is aligned along the positive z-axis, $\theta_3 = \theta_{23}$, $\theta_4 = \theta_{34}$, $r_{ij} = \sqrt{r_i^2 + r_j^2 - 2r_i r_j \cos\theta_{ij}}$, and $\cos\theta_{34} = \cos\theta_3 \cos\theta_4 + \sin\theta_3 \sin\theta_4 \cos\phi_{34}$. This equation is simplified by expansion in Legendre polynomials of the angularly dependent function in the integrand and by using well-known algebraic manipulations. The result is an expression in terms of the coefficients of the expansion [2, 7, 8, 10]. When the coefficients are expressed by

$$\hat{f}_n(r_i, r_j) = \frac{2n+1}{2} \int_{-1}^{1} P_n(x) f\left(\sqrt{r_i^2 + r_j^2 - 2r_i r_j x}\right) \mathrm{d}x \quad (18)$$

for $x = \cos\theta$, the final expression for our integral becomes

$$d_3(r_{12}) = 2\pi^2 \sum_{n=0}^{\infty} \left(\frac{2}{2n+1}\right)^2 \int_0^{\infty} r_3^2 f(r_{13}) \mathrm{d}r_3 \times \int_0^{\infty} r_4^2 f(r_{14}) \hat{f}_n(r_2, r_3) \hat{f}_n(r_2, r_4) \hat{f}_n(r_3, r_4) \mathrm{d}r_4 \ . \quad (19)$$

Note that we have two different orders of polynomial inherent in the evaluation of this last integral; namely, the order used to evaluate the coefficients of the expansion $\hat{f}_n(r_i, r_j)$ and the independent order necessary to integrate over the radial variables r_3 and r_4, which arises from the use of Gaussian quadrature to perform the radial integrations. The orders of these polynomials become a point of interest in the numerical solution. This will be more fully illustrated in Sect. 3, where we discuss the numerical results of the integrals which appear in this section. We will report the virial coefficients in units reduced by $b_0 = 2\pi\sigma^3/3$ and denote them as $D_1^* = D_1/b_0^3$, with similar reductions for D_2, D_3, and D.

All calculations will employ the Lennard-Jones potential [4] defined by

$$u(r) = 4\epsilon\left[\left(\frac{\sigma}{r}\right)^{12} - \left(\frac{\sigma}{r}\right)^{6}\right] \ , \quad (20)$$

where ϵ and σ are the standard well depth and distance parameters.

2.3 Direct expansion of the fourth-order virial coefficients

Direct expansion of the virial coefficients was first given by Mayer and Harrison [14]. This direct expansion in terms of the Mayer f bond has been by far the most common method of calculation of the virial coefficients [6, 7, 8, 11, 12, 14, 15], predominately owing to the fact that this expansion has been shown to be more appropriate when approximations are necessary to complete a calculation [12, 15]. We defer discussion of the reasoning for this viewpoint to the end of this section, where we detail the equivalence of the alternative methods reviewed in this work. For now, we merely state the expansion of the fourth-order coefficient and outline our method of calculation. We have followed the method outlined by Barker and coworkers [6, 7, 8].

The virial equation as given by Mayer takes the form

$$\frac{\beta P}{\rho} = 1 - \sum_{n\geq 1} \frac{n}{n+1} \Gamma_n \rho^n \ , \quad (21)$$

where

$$\Gamma_n = \frac{1}{n!} \int_n \cdots \int \sum \Pi f(r_{ij}) \mathrm{d}\mathbf{r}_2 \cdots \mathrm{d}\mathbf{r}_n \ . \quad (22)$$

Γ_n, the virial coefficients, are then sums over products of the f bonds in $n+1$ points.

From Eqs. (21) and (22), we have that the fourth-order coefficients,

$$\Gamma_3 = D = -\frac{3}{4} \cdot \frac{1}{3!} [3(D_1) + 6(D_2) + D_3] \ , \quad (23)$$

are given by the integrals

$$D_1 = -\frac{3}{8} \int\int\int f(r_{12}) f(r_{14}) f(r_{23}) f(r_{34}) \mathrm{d}\mathbf{r}_2 \, \mathrm{d}\mathbf{r}_3 \, \mathrm{d}\mathbf{r}_4 \ , \quad (24)$$

$$D_2 = -\frac{6}{8} \int\int\int f(r_{12}) f(r_{13}) f(r_{13}) f(r_{23}) f(r_{34}) \times \mathrm{d}\mathbf{r}_2 \, \mathrm{d}\mathbf{r}_3 \, \mathrm{d}\mathbf{r}_4 \ , \quad (25)$$

$$D_3 = -\frac{1}{8} \int\int\int f(r_{12}) f(r_{13}) f(r_{14}) f(r_{23}) f(r_{24}) f(r_{34}) \times \mathrm{d}\mathbf{r}_2 \, \mathrm{d}\mathbf{r}_3 \, \mathrm{d}\mathbf{r}_4 \ , \quad (26)$$

where the integral fraction in D_2 has been left unreduced to highlight the numerators in the integrals. These integers, 3, 6, and 1, indicate the symmetry number of the labeled diagrams D_1, D_2, and D_3, respectively; alternatively, these symmetry numbers can be seen as the number of equivalent pairwise index permutations with respect to the f bond which can be performed under the integral. The diagrams which represent these integrals are given in Fig. 2.

We begin our reduction of the integrals by expanding D_3 in angular coordinates to get

$$D_3 = -\pi^2 \int_0^{\infty} r_2^2 \, \mathrm{d}r_2 \int_0^{\infty} r_3^2 \, \mathrm{d}r_3 \int_0^{\infty} r_4^2 \, \mathrm{d}r_4 \times \int_0^{\pi} \sin\theta_{23} \, \mathrm{d}\theta_{23} \int_0^{\pi} \sin\theta_{34} \, \mathrm{d}\theta_{34} \times \int_0^{2\pi} f(r_{12}) f(r_{13}) f(r_{14}) f(r_{23}) f(r_{24}) f(r_{34}) \ . \quad (27)$$

By again applying Eq. (18) and expanding in Legendre polynomials, we find that

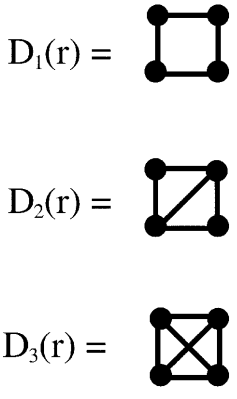

Fig. 2. The diagrammatic expansion of D_1, D_2, and D_3

$$D_3 = -8\pi^3 \sum_{n=0}^{\infty} \left(\frac{2}{2n+1}\right)^2 \int_0^{\infty} f(r_2) r_2^2 \, \mathrm{d}r_2 \int_0^{\infty} f(r_3) r_3^2 \, \mathrm{d}r_3 \times \int_0^{\infty} f(r_4) r_4^2 \hat{f}_n(r_2, r_3) \hat{f}_n(r_2, r_4) \hat{f}_n(r_3, r_4) \mathrm{d}r_4 \ . \quad (28)$$

It is easy to see that this may be further reduced by noting that

$$D_3 = -4\pi \int_0^{\infty} f(r_2) r_2^2 \, \mathrm{d}r_2 \times d_3(r_{12}) \ , \quad (29)$$

where $d_3(r_{12})$ is defined in Eq. (19). Thus, the numerical evaluation of the bridge diagram of the virial expansion follows exactly the evaluation of $d_3(r_{12})$, which was detailed earlier.

The reduction of D_1 and D_2 to more tractable form may take either of two distinct paths. One method would be to evaluate them as convolution integrals, in an analogous manner to $d_1(r_{12})$ and $d_2(r_{12})$ [11]. The second method, which we will follow in our stated purpose of showing numerical convergence independent of the method, follows a similar expansion in angular coordinates as that of the bridge diagram. The full derivation can be found elsewhere [6, 7]; here, we state the results. Specifically, if we define

$$\frac{\zeta(r_j)}{r_j} = \int_0^{\infty} f_i r_i^2 \, \mathrm{d}r_i \times \int_0^{\pi} f\left(\sqrt{r_i^2 + r_j^2 - 2 r_i r_j \cos\theta_{ij}}\right) \sin\theta_{ij} \, \mathrm{d}\theta_{ij} \ , \quad (30)$$

then it follows that

$$D_1 = -6\pi^3 \int_0^{\infty} [\zeta(r)]^2 \mathrm{d}r \quad (31)$$

$$D_2 = -12\pi^3 \int_0^{\infty} f(r)[\zeta(r)]^2 \mathrm{d}r \ . \quad (32)$$

The numerical approach to these equations can be resolved by noting that

$$\zeta(r_j) = \int_0^{\infty} f(r_i) r_i \, \mathrm{d}r_i \times \hat{f}_0(r_i, r_j) \ . \quad (33)$$

Thus, the evaluation of D_1 and D_2 reduces to the evaluation of the first term in the expansion $\hat{f}_n(r_i, r_j)$. For the evaluation of the $\hat{f}_0$ term, in this sense completely separated from the calculation of the bridge diagrams, we calculate this term through the use of a Romberg integration scheme [16] rather than the Gaussian integration used to evaluate these coefficients in the bridge diagram computation. For notational purposes, from this point we will refer to the virial coefficients calculated through this direct method as D_1(Barker), etc.

2.4 Note on the equivalence of the two methods

The equivalence of the expansion of the virial coefficients directly as irreducible integral functions of the f bond, and as expansions of the radial distribution function, has been the main stumbling point in the comparison of the two methods. Specifically, it has been shown [15] that the two are equivalent only when all diagrams forming an exact expression for $g(r)$ have been accounted for. For this reason, previous work has concentrated upon the direct expansion. The inclusion of an accurate calculation of the bridge diagram in the $g(r)$ expansion [2, 10] now allows a clearer comparison of the two methods.

We recall the different definitions which we have given for the virial equation, i.e.

$$\frac{\beta P}{\rho} = 1 - \frac{2}{3}\pi\beta\rho \int_0^{\infty} r^3 g(r) \frac{\mathrm{d}u(r)}{\mathrm{d}r} \mathrm{d}r \quad (34)$$

and

$$\frac{\beta P}{\rho} = 1 - \sum_{n \geq 1} \frac{n}{n+1} \Gamma_n \rho^n \ , \quad (35)$$

where

$$g(r) = \mathrm{e}^{-\beta u(r_{12})}\left[1 + \rho g_1(r_{12}) + \rho^2 g_2(r_{12}) + \cdots\right] = \mathrm{e}^{-\beta u(r_{12})}\left[1 + \sum_{n \geq 1} g_n(r) \rho^n\right] \quad (36)$$

for

$$g_n(r) = \frac{1}{n!} \int_n \cdots \int \sum \Pi f(r_{ij}) \mathrm{d}\mathbf{r}_3 \cdots \mathrm{d}\mathbf{r}_n \ , \quad (37)$$

and

$$\Gamma_n = \frac{1}{n!} \int_n \cdots \int \sum \Pi f(r_{ij}) \mathrm{d}\mathbf{r}_2 \cdots \mathrm{d}\mathbf{r}_n \ . \quad (38)$$

Note that there are $n+1$ vertices in Γ_n and $n+2$ vertices in $g_n(r)$. Formal equivalence of the two variations, Eqs. (34) and (35), has been proven by Rushbrooke and Scoins [15] by substituting Eq. (36) into Eq. (34) to yield Eq. (35).

The proof of this shows equivalence of the expansions of the virial equation as a whole with term-by-term equality implied. Finally, we state that this equality holds in an isotropic, homogeneous medium for which the potential is pairwise-additive. The question of equality in more general cases must be shown on an individual basis and is not necessary here.

3 Results

The numerical results of our calculation of the fourth-order virial coefficients of the Lennard-Jones fluid have been summarized in Tables 1, 2, 3, 4, 5, and 6, and further illustrated in Figs. 3, 4, and 5. Our final results for D^* at phase points ranging from $T^* = 20.0$ to 0.625 are given in Table 1. The numbers are reported to the

Table 1. The reduced fourth-order virial coefficient of the Lennard-Jones potential over T^*

T^*	D_1^*	D_2^*	D_3^*	D^*
20.00	−0.23023	0.35384	−0.04036	0.08325
15.00	−0.25232	0.39453	−0.04553	0.09669
10.00	−0.27809	0.44613	−0.05245	0.11559
7.500	−0.29189	0.47537	−0.05664	0.12684
5.000	−0.30933	0.50420	−0.06075	0.13412
4.000	−0.32388	0.51684	−0.06184	0.13113
3.000	−0.36060	0.54223	−0.06182	0.11980
2.500	−0.40460	0.57857	−0.06084	0.11314
2.400	−0.41800	0.59118	−0.06048	0.11270
2.300	−0.43383	0.60689	−0.06003	0.11303
2.200	−0.45274	0.62668	−0.05947	0.11447
2.100	−0.47566	0.65193	−0.05875	0.11752
2.000	−0.50393	0.68461	−0.05783	0.12285
1.900	−0.53960	0.72756	−0.05659	0.13137
1.800	−0.58583	0.78502	−0.05489	0.14430
1.700	−0.64779	0.86341	−0.05246	0.16315
1.600	−0.73420	0.97274	−0.04884	0.18971
1.500	−0.86045	1.12908	−0.04316	0.22548
1.400	−1.05501	1.35895	−0.03377	0.27017
1.300	−1.37326	1.70747	−0.01729	0.31693
1.250	−1.61050	1.94896	−0.00438	0.33408
1.225	−1.75774	2.09231	0.00383	0.33842
1.150	−2.36493	2.64156	0.03899	0.31562
1.125	−2.64288	2.87465	0.05563	0.28740
1.100	−2.97270	3.13916	0.07573	0.24219
1.050	−3.83785	3.78208	0.12995	0.07418
1.000	−5.09685	4.61693	0.21182	−0.26810
0.950	−6.97328	5.70211	0.33855	−0.93262
0.875	−11.84166	7.93990	0.68415	−3.21761
0.800	−21.73146	10.96645	1.42735	−9.33767
0.750	−34.18448	13.03741	2.40234	−18.74473
0.625	−130.63139	−0.09749	10.17001	−120.55887

Table 2. The dependence of the virial coefficients calculated by the fast Fourier transform (*FFT*) method upon the number of points (*npts*) in the grid for $T^* = 1.2$

npts	dr	D_1^*	D_2^*
1024	0.00625	−1.928822065	2.253701524
2048	0.00625	−1.929110791	2.253703918
4096	0.00625	−1.929110959	2.253703923
8192	0.00625	−1.929110959	2.253703923

Table 3. Range convergence results at $T^* = 1.2$ for the coefficients calculated through the Barker method

npts	dr	D_1^*(Barker)	D_2^*(Barker)
1000	0.00750	−1.929088646	2.253679640
1100	0.00750	−1.929093271	2.253679789
1200	0.00750	−1.929094924	2.253679849
1300	0.00750	−1.929095575	2.253679875
1400	0.00750	−1.929095852	2.253679887
1500	0.00750	−1.929095978	2.253679893
1600	0.00750	−1.929096040	2.253679896

fifth decimal place and were calculated with 8192 points and a grid spacing of $\sigma/160$. These calculations show some deviation from the values reported in the literature [6, 11] at all points in the temperature regime; these

Table 4. The dependence of the virial coefficients calculated by the FFT method upon the spacing (dr), of the grid at $T^* = 1.2$

npts	dr	D_1^*	D_2^*
512	0.10000	−1.925723828	2.253693976
1024	0.05000	−1.929019015	2.253756058
2048	0.02500	−1.929110960	2.253703922
4096	0.01250	−1.929110959	2.253703923
8192	0.00625	−1.929110959	2.253703923

Table 5. Spacing convergence results at $T^* = 1.2$ for the coefficients calculated through the Barker method

npts	dr	D_1^*(Barker)	D_2^*(Barker)
50	0.15000	−1.899939740	2.136280493
100	0.07500	−1.917817050	2.230967692
200	0.03750	−1.927622020	2.250740427
400	0.01875	−1.928915164	2.253327265
800	0.00937	−1.929079940	2.253656448
900	0.00833	−1.929086714	2.253670585
1000	0.00750	−1.929092687	2.253680512
1100	0.00682	−1.929093527	2.253685592
1200	0.00625	−1.929096364	2.256898262
1300	0.00577	−1.929098543	2.253692375
1400	0.00536	−1.929099250	2.253693969
1500	0.00500	−1.929099148	2.253696586
1600	0.00469	−1.929099908	2.253697796

Table 6. Dependence of D_3^* at $T^* = 1.2$ on the order of the polynomials in the calculation

v_1	v_2	D_3^*	D_3^*(Barker)
4	16	0.1197250	−0.0601363
8	16	−0.1496790	−0.0368914
16	16	−0.1614550	−0.0180003
8	32	−0.0133230	−0.0179551
16	32	0.0428704	0.0282048
32	32	0.0539174	0.0265751
16	64	0.0163064	0.0136184
32	64	0.0143019	0.0139738
64	64	0.0143848	0.0139824
32	128	0.0135777	0.0135687
64	128	0.0135668	0.0135659
128	128	0.0135668	0.0135660
64	256	0.0135654	0.0135654
128	256	0.0135654	0.0135654

deviations lie in the third and fourth decimal place for most of the values reported , with some second decimal place discrepancies in the temperature region between $T^* = 1.4$ and 0.8. Deviation in this area should not be surprising, as it has been previously reported that this region corresponds to the area around the critical point for the Lennard-Jones fluid [7]. This result, as well as interest in the numerical behavior of the calculation, requires that we show convergence. To this end, we have provided convergence tables at $T^* = 1.2$ in Tables 3, 5, and 6 and plots of the convergence behavior of the various integrands in Figs. 3, 4, and 5.

Tables 2, 3, 4, 5, and 6 show the numerical dependence of the different methods; Tables 2, 3, 4, 5 give the

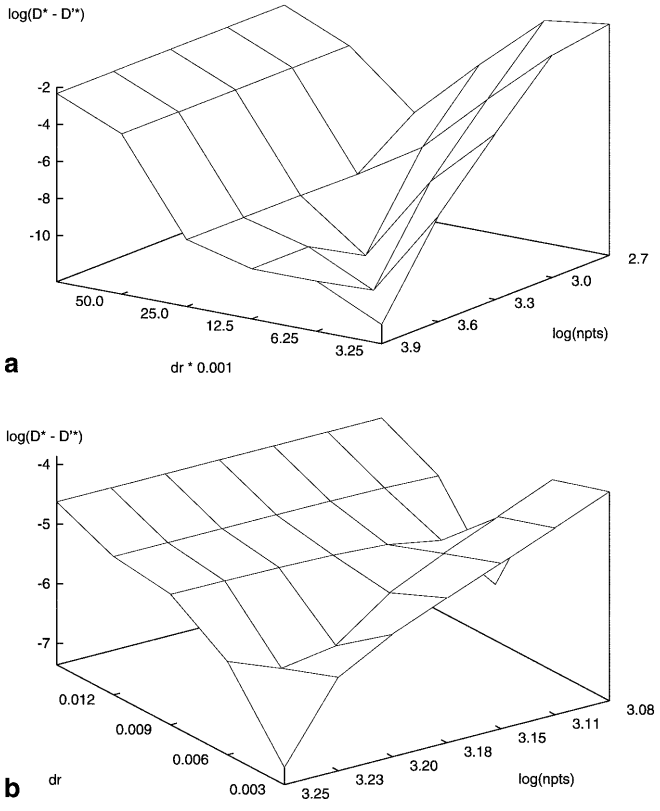

Fig. 3. **a** The convergence of D^* with respect to the logarithm of the number of points (*npts*) and the spacing of the grid (d*r*), as calculated in the method outlined in this article. **b** The convergence of D^* as calculated through the method given by Barker and coworkers

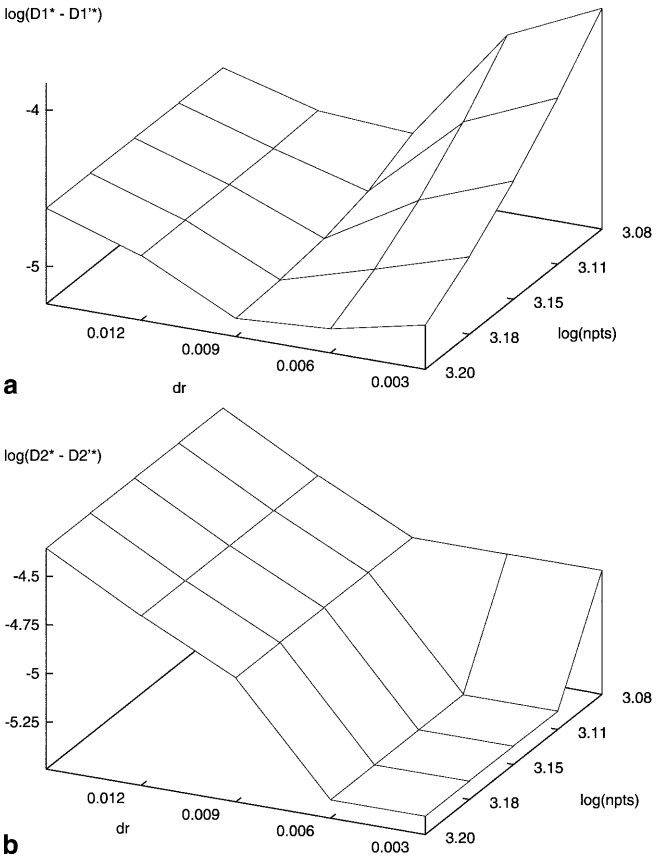

Fig. 4. **a** The convergence of D_1^*(Barker). **b** The convergence of D_2^*(Barker)

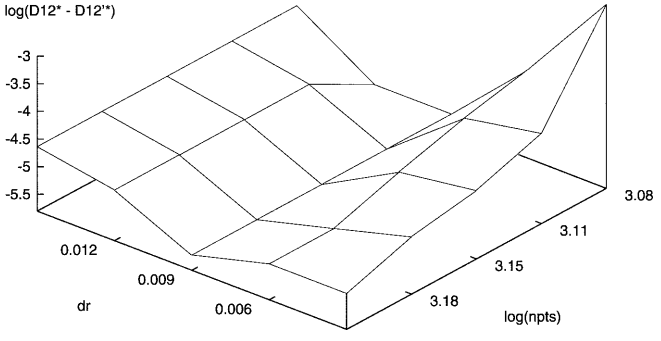

Fig. 5. The convergence of the sum D_1^*(Barker) + D_2^*(Barker) = D_{12}^*

convergence of D_1^* and D_2^* on the range and spacing of the grid, while Table 6 gives the dependence of D_3^* on the polynomial orders present in the calculation. The information given in these tables is necessary so that we may show convergence of the two methods, in a consistent manner as well as with respect to the other method; however, analysis and comparison leads to plots such as those given in Figs. 3, 4, and 5. In particular, when the total value of D^*, as given from both methods, is plotted on a convergence graph, such as is seen in Fig. 3a and b, analysis of the results becomes more straightforward. Figure 3a and b was plotted as the logarithm of the difference of the results of a calculation at a given point in the grid with the converged answer, i.e. $\log(D^* - D^{*\prime})$, versus the range and spacing of the grid. The resulting plot for the virial coefficient calculated using $g(r)$ is given in Fig. 3a, while the result from the calculation of the virial coefficient using the method of Barker is given in Fig. 3b. These plots show that the sum of the individual integrals does converge well and to the same answer regardless of the method. The differences between the two plots also gives us a chance to analyze the different numerical behavior of the two methods. In particular, a major feature of any such plots would be the range in which one would consider an answer to have reached the precision necessary: this feature takes the form of a groove within the graph. This groove is present within Fig. 3a and b, but has different characteristics for each. The groove in Fig. 3a is wide and well defined, indicating that a converged answer can be attained within a wide range of grid spacing. In contrast, the groove in Fig. 3b is ill defined and narrow and, furthermore, only reaches a converged answer at the very extreme of the grid, where extreme here is used to mean long range and small grid spacing. Another essential feature of such grooves can be seen in the smoothness of Fig. 3a with respect to Fig. 3b. Figure 3b shows features that do not appear in the case presented in Fig. 3a. In particular, there appears a ''premature'' dip corresponding to a converged answer, a rise to nonconvergence which then follows into a true

convergence groove. Analysis of this feature leads to the plots given in Figs. 4 and 5.

The convergence of D_1^*(Barker) and D_2^*(Barker) in a manner analogous to Fig. 3b is shown in Fig. 4a and b. These results, plotted separately, show no particular feature which should correspond to the premature convergence which appears in Fig. 3b; however, when the sum of the two integrals is plotted, as in Fig. 5, where the sum of the two integrals is denoted by D_{12}, what immediately becomes apparent is that there appears to be a rather fortuitous cancellation appearing at the corresponding area of Fig. 3b.

The results from this analysis of the D_1^*(Barker) and D_2^*(Barker) terms leads naturally to Tables 5 and 6, where we give the convergence of both methods of calculating D_3^*. The results of Figs. 4 and 5 show that the bridge diagram has more influence than would have been thought, especially in the critical region of the phase diagram. Furthermore, since this integral is the most difficult to calculate, regardless of the formal method used, the numerical techniques used must be applied with much care. Figures 4 and 5 also show that numerical precision must be maintained and shown for even the simple diagrams. Direct comparison of the results presented here with those in the literature [6, 11] must be taken with some thought, as no such individual analysis was done in the previous work; however, the fact that the literature results agree with those given here to a reasonable level of precision in the majority of the phase points indicates that most of the phase diagram, as previously calculated, remains accurate and precise to three decimal place precision. However, the region immediately surrounding the physically important and interesting critical region may be examined in the light of the work presented here.

Another factor of Figs. 3, 4, and 5 may be elucidated in terms of computational efficiency. Specifically, if we think of the acceptable regions of Fig. 3 in terms of computational ease, the smooth, wide groove of Fig. 3a becomes more attractive in these terms. This trend is further enhanced by the timing associated with each method of calculation. For example, the calculation of the total D^* using the FFT method required on average 18 min of computing time for a DEC-Alpha 2100-475 per phase point, while the calculation of the virial coefficients directly through the method of Barker required an average of 240 min for the 1600-point calculation at a particular phase point.

4 Conclusions

The fourth-order virial coefficient has been calculated exactly to five decimal places for pure Lennard-Jones fluids at many points in the phase diagram. The calculations included the standard Fourier transform method for evaluating the simply connected diagrams and the evaluation of the bridge diagram for the fourth order in density by expansion in Legendre polynomials, a method developed for hard spheres by Attard and Patey [2] and applied to Lennard-Jones fluids by Perkyns and Pettitt [10]. The polynomial-order dependence of the bridge diagram calculation and the range dependence of the simply connected diagrams of the fourth order were found to have more significance than was apparent from previous calculations [6, 7, 8, 17]. The more strenuous numerical tests performed demonstrate errors of larger size than were claimed in the literature [6, 7, 8, 11, 17]. This result was confirmed by comparison with calculation of the virial coefficients through direct expansion in irreducible cluster integrals, as has been previously shown in the literature [6, 7, 11]. Our calculations were also found to be quite well suited for modest workstations, with the evaluation in its entirety for one thermodynamic state being accomplished in approximately 18 min of computing time using a DEC-Alpha 2100-475.

The exact calculation of the virial coefficients to arbitrary accuracy denotes more than an interesting addendum to the theory of statistical mechanics; this type of calculation represents a necessary first step in the study of phase behavior, which when extended to more complex systems, will allow the prediction of thermodynamic quantities of fluids in previously intractable systems. Such quantities are of great current interest in biological [18] and engineering [1, 3, 5] fields and are as yet only obtainable by semiempirical approaches. Future study will require the ability to extend the distribution function methods presented here to ionic mixtures and molecular species.

Acknowledgements. The authors gratefully acknowledge the support of the Robert A. Welch Foundation.

References

1. Atkins P (1994) Physical chemistry, 5th edn, Freeman, New York
2. Attard P, Patey GN (1990) J Chem Phys 92: 4970
3. Barker JA, Henderson D (1972) Annu Rev Phys Chem 23: 439
4. Hansen JP, McDonald IR (1986) Theory of simple liquids, 2nd edn. Academic, London
5. McQuarrie DA (1973) Statistical mechanics. Harper and Row, New York
6. Barker JA, Leonard PJ, Pompe A (1966) J Chem Phys 44: 4206
7. Barker JA, Monaghan JJ (1962) J Chem Phys 36: 2564
8. Barker JA, Monaghan JJ (1962) J Chem Phys 36: 2558
9. Nijboer BRA, van Hove L (1952) Phys Rev 85: 777
10. Perkyns JP, Pettitt BM (1997) Theor Chem Acc 1: 61–70; ibid (1998) 99: 207–208
11. Sun T, Teja AS (1996) J Phys Chem 100: 17365
12. Rowlinson JS (1964) Proc R Soc Lond, Ser A 279: 147
13. Mayer JE, Mayer MG (1940) Statistical mechanics. Wiley, New York
14. Mayer JE, Harrison SF (1938) J Chem Phys 6: 87
15. Rushbrooke GS, Scoins HI (1953) Proc R Soc Lond, Ser A 216: 203
16. Press WH, Flannery BP, Teukolsky SA, Vetterling WT (1988) Numerical recipes in C: the art of scientific computing. Cambridge University Press, New York
17. Wakayama S, Koshi M, Matsui H (1991) Chem Soc Jpn 64: 3329
18. Perkyns JS, Pettitt BM (1996) J Am Chem Soc 118: 1164